Biophysical Journal, Volume *111*

Supplemental Information

Regulation of K-Ras4B Membrane Binding by Calmodulin

Benjamin Sperlich, Shobhna Kapoor, Herbert Waldmann, Roland Winter, and Katrin Weise

MATERIALS AND METHODS

Sample preparation

Stock solutions of 10 mg mL^{-1} lipid (DOPC, DOPG, DPPG, DPPC, Chol) in chloroform/methanol 4:1 for DPPG and chloroform for all other lipids were prepared and mixed to obtain 1.94 mg of total lipid with the composition of DOPC/DOPG/DPPC/DPPG/Chol 20:5:45:5:25 (mol%). The majority of the chloroform was evaporated with a nitrogen stream and all solvent was subsequently removed by drying under vacuum overnight. All buffers were filtered through filters of 0.02 µm pore size (Whatman, Dassel, Germany) before use. The dry lipid film was resuspended with 1 mL of 10 mM Hepes, 5 mM $MgCl_2$, 150 mM NaCl, 1 mM $CaCl_2$, pH 7.4 for the SPR or 20 mM Tris, 7 mM $MgCl_2$, 1 mM $CaCl_2$, pH 7.4 for the AFM and fluorescence spectroscopy experiments to yield a total lipid concentration of 3 mM. Afterwards, the lipid mixture was vortexed, kept in a water bath at 65 °C for 15 min, and sonicated for 10 min. After five freeze-thaw-vortex cycles and brief sonication, large multilamellar vesicles were formed and transformed to large unilamellar vesicles (LUVs) of uniform size by use of an extruder (Avanti Polar Lipids, Alabaster, USA) with polycarbonate membranes of 100 nm pore size at 65 °C (1,2). The extruded lipid solution was further diluted to a concentration of 0.5 mM for SPR experiments.

Atomic force microscopy

Vesicle fusion on mica was carried out by depositing 35 µL of the extruded lipid vesicle solution together with 35 µL of Tris buffer (20 mM Tris, 7 mM $MgCl_2$, 1 mM $CaCl_2$, pH 7.4) on freshly cleaved mica (NanoAndMore, Wetzlar, Germany) and incubation in a wet chamber at 70 °C for 2 h. After vesicle fusion, the samples were rinsed carefully with Tris buffer to remove excess unspread lipid vesicles (1,2). For the protein–membrane interaction studies, 800 µL of either K-Ras4B ($c_{K\text{-}Ras4B}$ = 0.2 µM), calmodulin (c_{CaM} = 0.3 µM) or K-Ras4B–Ca^{2+}/CaM (0.2 µM / 0.3 µM) in Tris buffer were slowly injected into the AFM fluid cell and allowed to incubate for 1 h at room temperature. Afterwards, the AFM fluid cell was rinsed carefully with Tris buffer to remove unbound protein. Measurements were performed at room temperature on a MultiMode scanning probe microscope with a NanoScope IIIa controller (Digital Instruments (now Bruker), Santa Barbara, CA, USA) and usage of a J-Scanner (scan size 125 µm). Images were obtained by applying the tapping mode in liquid with sharp nitride lever (SNL) probes mounted in an AFM fluid cell (MTFML, both Veeco (now Bruker), Mannheim, Germany). Tips with nominal force constants of 0.24 N m^{-1} were used at driving frequencies around 9 kHz and drive amplitudes between 200 and 400 mV. Scan frequencies were between 1.0 Hz and 2.0 Hz. Height and phase images with resolutions of 512 × 512 pixels were analyzed using the image analysis and processing software NanoScope version 5 and 6 (Veeco (now Bruker), Mannheim, Germany) and Origin 8.6 (OriginLab, Northampton, USA).

Surface plasmon resonance

SPR experiments were carried out with a Biacore 3000 system (Biacore, Uppsala, Sweden; now GE Healthcare, Freiburg, Germany). For the protein-membrane interaction studies, the L1 sensor chip (GE Healthcare, Freiburg, Germany) was used, which is composed of a thin lipophilic modified dextran matrix on a gold surface, upon which lipid bilayers can be immobilized through the capture of liposomes by the lipophilic compounds. The chip has been shown to be suitable for the generation of model membrane systems that provide a flexible lipid bilayer surface that closely resembles the surface of a cellular membrane. All measurements were carried out at a temperature of 25 °C, with the samples cooled at 10 °C in the autosampler before the measurements were started. Prior to the experiment, the L1 chip was primed 4× with Hepes buffer (10 mM Hepes, 5 mM $MgCl_2$, 150 mM NaCl, 1 mM $CaCl_2$, pH 7.4). Afterwards, the chip surface underwent a cleaning program by injecting

30 μL 2-propanol / 50 mM NaOH (2:3), 10 μL octyl β-D-glucopyranoside (40 mM), and 30 μL Chaps (20 mM), NaCl (100 mM), and $CaCl_2$ (20 mM) at a flow rate of 5 μL/min. For the vesicle immobilization, 15 μL of the extruded lipid vesicle solution (0.5 mM) were injected twice at a flow rate of 2 μL/min, which was followed by a stabilization phase by injecting 50 μL of Hepes buffer at a flow rate of 100 μL/min and three further injections of 10 μL 25 mM NaOH at a flow rate of 5 μL/min. Finally, the lipid surface was stabilized by injecting 40 μL Hepes buffer at a flow rate of 20 μL/min. After baseline stabilization, 40 μL of the protein containing solution ($c_{\text{K-Ras4B}}$ = 2 μM, c_{CaM} = 3 μM) were injected at a flow rate of 20 μL/min and the dissociation was followed for 30 min. Next the chip surface was regenerated using the cleaning program. The degree of chip surface coverage with lipids was determined by means of 0.5 μM BSA and was found to be ≥75% for all cases. To eliminate unspecific binding effects such as the interaction of Hepes buffer with the L1 chip and nonspecific binding of the proteins to the pure L1 chip that depend on the determined lipid coverage, these signals were subtracted from the actual sensorgrams of the respective protein solutions. Hence, the ratio of the maximal amplitude of the BSA-membrane and BSA-chip sensorgram yields the amount of the chip surface that is not covered with lipids and is used as a factor for correcting the zeroized (i.e., setting the baseline before injection of the protein solution to zero) protein-chip sensorgram. This corrected sensorgram is then subtracted from the buffer corrected and zeroized protein-membrane sensorgram to yield the final protein-membrane sensorgram for analysis. All sensorgrams were recorded at a frequency of 10 Hz.

For all measurements performed, the SPR data were analyzed on the basis of a multi-step model owing to the non-simple-exponential association and dissociation curves observed in the sensorgrams for the protein-membrane interaction, reflecting a complex interaction behavior. A two-step reaction model was shown to provide an appropriate curve-fitting algorithm and describes a process with two reaction steps that, in terms of protein-lipid interactions, correspond to:

$$\mathrm{P} + \mathrm{L} \underset{k_{\text{off},1}}{\overset{k_{\text{on},1}}{\rightleftharpoons}} \mathrm{PL} \underset{k_{\text{off},2}}{\overset{k_{\text{on},2}}{\rightleftharpoons}} \mathrm{PL}^{*} \qquad \text{(Scheme S1)}$$

where the soluble protein (P) binds to the immobilized lipids (L) forming a primary binding complex (PL) and a secondary protein-lipid complex (PL*, e.g. a clustered state as shown for K-Ras4B by atomic force microscopy) after relocation of protein and lipid molecules within the lipid bilayer plane. The effect of the K-Ras4B clustering on the response measured is indirect in altering the equilibrium between the bound and free forms of the protein, allowing a dissociation of PL* only through reversal of the clustering reaction step. To directly obtain values for the association rate constant k_{on}, the whole sensorgram was fitted to the two-step model. Curve fitting was performed by using the Marquardt-Levenberg algorithm and the fitted curves were generated by numerical integration of the differential equations that describe the reaction scheme. This fitting procedure was implemented in the BIAevaluation software 4.1 (Biacore, Uppsala, Sweden). Whereas the two-step fit of the whole sensorgram gave reasonable results for the association phase, a larger discrepancy was observed for the fitted dissociation part of the curve. Thus, the dissociation phase was fitted separately to a biexponential model (Eq. S1) using Origin 8.6, yielding two independent dissociation rate constants $k_{\text{off},1}$ and $k_{\text{off},2}$ as well as their respective contributions A_1 and A_2.

$$R = A_1 \cdot e^{-k_{\text{off},1}(t-t_0)} + A_2 \cdot e^{-k_{\text{off},2}(t-t_0)} + \text{offset} \qquad \text{(S1)}$$

t_0 indicates the beginning of the dissociation phase, i.e., the time point when the flow cell switched from protein to buffer solution. The relative amount of quasi-irreversibly bound protein was derived by correlating the offset value of the biexponential fit to the initial amplitude at the starting point (t = 0) of the dissociation phase corresponding to the following equation:

$$\text{quasi} - \text{irrevers.} = \frac{\text{offset}}{A_1 + A_2 + \text{offset}}. \quad \text{(S2)}$$

The model and the corresponding analysis have been described in detail before (1,3).

Infrared reflection absorption spectroscopy

All experiments were performed with a Wilhelmy film balance (Riegler, Berlin, Germany) using a filter paper as Wilhelmy plate. Two teflon troughs of different sizes were linked by two small bores to ensure equal heights of the air-D_2O interface in both troughs. The temperature of the subphase was maintained at 20 ± 0.5°C and measurements were performed in the small (reference) trough at constant surface area. A Plexiglas hood covered the entire reflection attachment to minimize the evaporation of subphase. Both troughs were filled with 20 mM Tris, 7 mM $MgCl_2$, 1 mM $CaCl_2$, pD 7.4. Monolayers of DOPC/DOPG/DPPC/DPPG/Chol 20:5:45:5:25 (mol%) were formed by directly spreading the lipid solution (1 mM) in a mixture of chloroform and methanol (3:1) onto the subphase. Protein measurements were performed by injecting the concentrated protein solution into the aqueous subphase underneath the lipid monolayer to yield a final concentration of K-Ras4B and Ca^{2+}/CaM of 200 and 300 nM, respectively.

Infrared spectra were recorded using a Vertex 70 FT-IR spectrometer (Bruker, Germany) connected to an A511 reflection attachment (Bruker) with an MCT detector using the trough system described above (4). The IR beam is focused by several mirrors onto the subphase and the trough system was positioned on a movable platform to be able to shuttle between sample and reference troughs. This shuttle technique diminishes the spectral interference due to water vapour absorption in the light beam. Parallel polarized light at an angle of incidence of 35° was used for recording of the IRRA spectra. All spectra were recorded at a spectral resolution of 8 cm^{-1} using Blackman-Harris-3-term apodization and a zero filling factor of 2. For each spectrum 2000 scans were co-added. The single beam reflectance spectrum of the large trough was ratioed as background (R_o) to the single beam reflectance spectrum of the lipid monolayer on the reference trough (R) to calculate the reflection absorption spectrum as $-\log(R/R_o)$.

Transmission Fourier-Transform infrared spectroscopy

For the transmission infrared spectroscopic experiments, the dry lipid mixture was hydrated with 100 μL of 20 mM Tris, 7 mM $MgCl_2$, pD 7.4, sonicated at 70 °C for 10 min and subsequently subjected to five freeze-thaw-vortex cycles. Afterwards, unilamellar vesicles of homogeneous size were obtained by using an extruder (Avanti Polar Lipids, Alabaster, AL) with polycarbonate membranes of 100 nm pore size at 70 °C. For the protein-lipid interaction studies, the GDP- and GTP-loaded K-Ras4B protein (m = 100 μg) was lyophilized for 3 h to remove H_2O and afterwards 20 μL of the freshly extruded lipid mixture were added ($c_{K\text{-}Ras}$ = 233 μM). The FT-IR cell was then assembled and spectra collection started.

Measurements were performed at 25 °C with a Nicolet 5700 FT-IR spectrometer equipped with a liquid nitrogen cooled MCT (HgCdTe) detector and a cell with CaF_2 windows that are separated by 50 μm mylar spacers. The spectrometer was purged continuously with dry air to remove water vapor. Typically, FT-IR-spectra of 128 scans were taken with a resolution of 2 cm^{-1} and corresponding processing was performed using GRAMS software (Thermo Electron). After background subtraction, the spectra were baseline corrected and normalized by setting the area between 1700 and 1600 cm^{-1} to 1 to allow for a quantitative analysis of the time evolution of secondary structural changes.

For the analysis of the secondary structure changes, second derivative and Fourier self-deconvolution (FSD) were applied to the normalized spectra to identify the components of the amide-I′ band region. These peaks were then fitted to the normalized raw spectra using a Levenberg-Marquardt curve fitting routine with bands of Voigt line shape. All spectra were

fitted with similar set of peaks and parameters. In ambiguous cases (such as the overlap of unordered and α-helical band regions), information from NMR and X-ray diffraction was taken into account. The area under each peak represents the fraction of the respective component (assuming similar transition dipole moments for the different conformers) and was finally used to determine the percentages of the secondary structure components.

Fluorescence anisotropy

Frequency-domain fluorescence anisotropy measurements were performed on a K2 multifrequency phase and modulation fluorometer (ISS Inc., Champaign, IL, USA). The temperature was maintained at 25 °C and controlled with an accuracy of ±0.1 °C using a circulating water bath. Time-resolved fluorescence lifetime and anisotropy measurements were performed in the frequency-domain using the cross-correlation technique (5,6). Excitation of dansyl-labeled CaM was accomplished by use of a 370 nm laser diode (ISS Inc., Champaign, IL, USA; with 370 $\pm$ 10 nm excitation filter) directly connected to a function generator, yielding intensity-modulated excitation light over a frequency range of 2–173 MHz at a cross-correlation frequency of 400 Hz. For modulation, a RF signal of +13 dBm was used. The dansyl emission was collected through a 400 nm long-pass filter. Fluorescence lifetime measurements at magic-angle conditions have been performed prior to the anisotropy experiments in 5 mm path-length quartz cuvettes. The excitation light was vertically polarized (0°), while the emission polarizer was set to an angle of 54.7°. The fluorescence of POPOP was used as lifetime reference (τ = 1.35 ns in ethanol). For the anisotropy experiments, the excitation light was vertically polarized, whereas the polarized emission components were recorded at polarization angles of 0° and 90°. The corresponding phase and modulation data were measured as a function of the modulation frequency.

In frequency-domain lifetime measurements, the shape of the frequency response is determined by the number of decay times displayed by the sample. Since the frequency response is not simple, a single-exponential decay is not sufficient for analysis of the data. Dansyl-labeling of CaM was performed by covalently attaching the dansyl group of dansyl chloride to a lysine residue of CaM. However, it can also react with the phenol group of tyrosine. Thus, the fluorescence lifetime of the dansyl group is different for the sulfonamide or sulfate binding type since it strongly depends on solvent polarity. Based on that, a biexponential decay of dansyl-labeled CaM can be explained by either dansyl groups that were located at two different lysines or bound to lysine and tyrosine. However, for proper analysis – especially when working with large unilamellar lipid vesicles – scattered light has also to be taken into account. Therefore, the phase angle and modulation data obtained in the fluorescence lifetime measurements were fitted using a triexponential decay model that includes two discrete lifetime components for dansyl-CaM and a discrete component fixed at 0.01 ns to account for scattered light:

$$I(t) = \alpha_1 \exp(-t/\tau_1) + \alpha_2 \exp(-t/\tau_2) + \alpha_3 \exp(-t/\tau_3), \quad \text{(S3)}$$

in which τ_1, τ_2, and τ_3 are the fluorescence lifetimes and the pre-exponentials α_1, α_2, and α_3 are the corresponding amplitudes. Thereby, τ_1 was fixed at 0.01 ns to account for scattered light. Nevertheless, the amount accounting for scattered light is rather small in all measurements ($\leq$ 8%). Fits were performed with phase delay errors and modulation ratio errors set to 0.20° and 0.0040, respectively. From the parameters obtained the average fluorescence lifetime, $\langle\tau\rangle$, of the dansyl label can be calculated:

$$\langle \tau \rangle = f_1\tau_1 + f_2\tau_2 + f_3\tau_3 , \quad \text{(S4)}$$

with f_1, f_2, and f_3 indicating the fractional contributions, which can be calculated from fluorescence lifetimes and the corresponding amplitudes by using the following equation:

$$f_i = \alpha_i \tau_i / \sum_i \alpha_i \tau_i \, . \qquad \text{(S5)}$$

The quality of the fit over the entire frequency range was determined by a nonlinear least squares algorithm and reduced χ^2 values were obtained in a range from 1 to 10. Representative fits are given in Fig. S5.

For anisotropy decay determination, differential polarized phase angles and modulation ratios were fitted to a biexponential model:

$$r(t) = r_0\left[g_1 \cdot \exp\left(-t/\theta_1\right) + g_2 \cdot \exp\left(-t/\theta_2\right)\right] = r_{0,1} \cdot \exp(-t/\theta_1) + r_{0,2} \cdot \exp(-t/\theta_2) \;, \qquad \text{(S6)}$$

in which r_0 is the maximum anisotropy. θ_1 and θ_2 account for the reorientational times of the dansyl label (being related to the segmental motion of the label) and the overall rotation of the protein that is equivalent to the overall rotational correlation time, θ_{protein}, of dansyl-labeled Ca^{2+}/CaM. The parameter g_1 and g_2 are the associated fractional amplitudes of each component in the anisotropy decay ($g_1 + g_2 = 1$), with $r_{0,1} = r_0 \cdot g_1$ and $r_{0,2} = r_0 \cdot g_2$. In the fitting process, the previously obtained lifetime data were entered as fixed parameters (cf. Table S1). Fits were performed with delta phase errors and amplitude ratio errors set to 0.20° and 0.0040, respectively. Reduced χ^2 values were obtained in a range of 0.3 to 5.4. Representative fits are given in Fig. S6. Experimental errors were calculated from at least three independent experiments and experimental data were fitted with the VINCI analysis software (ISS Inc., Champaign, IL, USA).

For the protein measurements in solution, dansyl-Ca^{2+}/CaM was diluted with Tris buffer (20 mM Tris, 5 mM $MgCl_2$, 1 mM $CaCl_2$, pH 7.4) to yield a final concentration of 3 μM. First, lifetime and anisotropy data of the protein were measured in the absence of K-Ras4B. Second, K-Ras4B was added in a 1.5 molar ratio ($c_{\text{K-Ras4B}}$ = 2 μM) to the dansyl-labeled Ca^{2+}-loaded CaM and the solution was allowed to incubate for 15 min. Finally, anionic lipid raft vesicles (LUVs composed of DOPC/DOPG/DPPC/DPPG/Chol 20:5:45:5:25 mol%) were added to the K-Ras4B/Ca^{2+}/CaM solution and allowed to incubate for 45 min, yielding a lipid concentration of 0.4 mM (lipid/K-Ras4B ratio of 200:1). Lifetime and anisotropy data were determined for dansyl-Ca^{2+}/CaM after every incubation step. According to the (rotational) Stokes−Einstein relation, the rotational correlation time, θ_{protein}, determined experimentally is proportional to the size (hydrodynamic volume) of the fluorescent protein, i.e., the danysl-labeled Ca^{2+}/CaM. Since the detected value of θ = 9.4 ns for dansyl-labeled Ca^{2+}/CaM in buffer solution (cf. Fig. 4 and Table S2) is significantly larger than that calculated for an equivalent hydrated spherical protein with a molecular volume of 32.4 nm^3 (θ = 7.0 ns) (7), a nonspherical form of monomeric Ca^{2+}-bound CaM has to be assumed, which is in agreement with its known dumbbell shape. The molecular weight is 17 kDa for dansyl-CaM and 21 kDa for K-Ras4B.

RESULTS

Lateral segregation of K-Ras4B and CaM in heterogeneous membranes

To gain complementary spatial information on the single molecule level with an imaging technique, time-lapse tapping mode atomic force microscopy (AFM) experiments were carried out. The protein−membrane interaction process was followed by imaging the same membrane region at various time points. Formation of a coherent, defect-free anionic lipid raft membrane on mica has been assured before addition of protein (cf. Figs. S8 and S9). The solid-supported lipid bilayer segregates into liquid-ordered (l_o) and liquid-disordered (l_d) domains at ambient conditions, which is characterized by a height difference of the two phases of about 1.0 nm (8,9) (Fig. S7).

To assess the membrane extraction process, at first K-Ras4B was added to the membrane, followed by subsequent addition of Ca^{2+}/CaM (Fig. S8). Thereby, protein-enriched domains could be observed within the l_d phase for both GDP- and GTP-bound K-Ras4B (Fig. S8 *B* and *E*, respectively). A mean height of the protein clustered domains of 1.0 ± 0.2 nm and 1.4 ± 0.3 nm with respect to the pure l_d phase was determined for K-Ras4B GDP and K-Ras4B GTP, respectively. These values are in agreement with previous AFM studies of our group that focused on the membrane localization of K-Ras4B (1,2). In analogous measurements of Ca^{2+}/CaM, no significant amount of protein could be detected in the membrane, indicating that Ca^{2+}/CaM does not bind to the anionic lipid raft membrane (Fig. S9 panels *E* and *F*). After injection of Ca^{2+}/CaM solution into the AFM fluid cell containing the K-Ras4B loaded membrane, no substantial changes could be observed for the membrane binding of both K-Ras4B GDP and K-Ras4B GTP (Fig. S8 *C* and *F*, respectively). The mean thickness of the K-Ras4B-enriched domains was also not considerably affected by addition of Ca^{2+}/CaM (K-Ras4B GDP: 1.6 ± 0.3 nm; K-Ras4B GTP: 1.8 ± 0.4 nm). Hence, these results suggest that Ca^{2+}/CaM cannot release K-Ras4B from solid-supported lipid membranes to a significant extent, which might be, for example, due to an effect of the solid support on the immobilized lipid bilayer, since the membrane-support separation is only 0.5–2.0 nm in buffer solution. This could induce steric constraints that might impede the displacement of the proteins. Generally, lower diffusion coefficients are detected in solid-supported membranes as compared to free-standing lipid bilayers of the same composition. Moreover, the large K-Ras4B clusters observed under these conditions in the AFM images may restrict efficient binding of Ca^{2+}/CaM to membrane-anchored K-Ras4B and thus impede K-Ras4B membrane extraction.

However, when the complex of K-Ras4B and Ca^{2+}/CaM, which was preformed in solution, was added to the anionic lipid raft membrane, the AFM images showed a considerably lower amount of K-Ras4B clusters (Fig. S9 *B* and *D*). This indicates that Ca^{2+}/CaM is able to bind K-Ras4B in solution and obstructs binding of K-Ras4B to the membrane, independent of the nucleotide state of K-Ras4B. Corroborated by the IRRAS and fluorescence anisotropy experiments, which also revealed no membrane interaction of the K-Ras4B–Ca^{2+}/CaM complex, we can conclude that binding of the strongly negatively charged Ca^{2+}/CaM to the polybasic stretch of K-Ras4B reverses its charge, preventing binding of the complex to the anionic model raft membrane due to repulsive interactions.

FIGURES

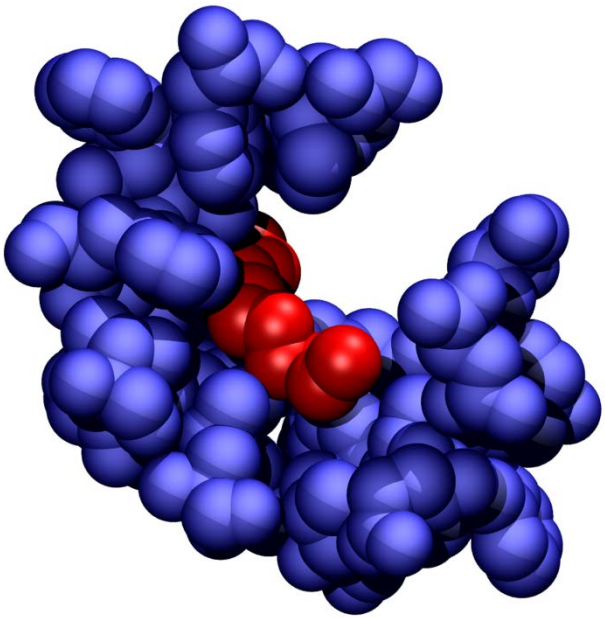

FIGURE S1 Binding interface of the myristoyl group in the hydrophobic tunnel of the CaM complex (PDB code: 1L7Z). Each atom of the corresponding Ca^{2+}/CaM residues is represented by a blue sphere scaled to its van der Waals radius. The volumetric distribution is shown within a distance of 7 Å; the myristoyl group is displayed in red. The image was generated by use of the molecular visualization program VMD (10).

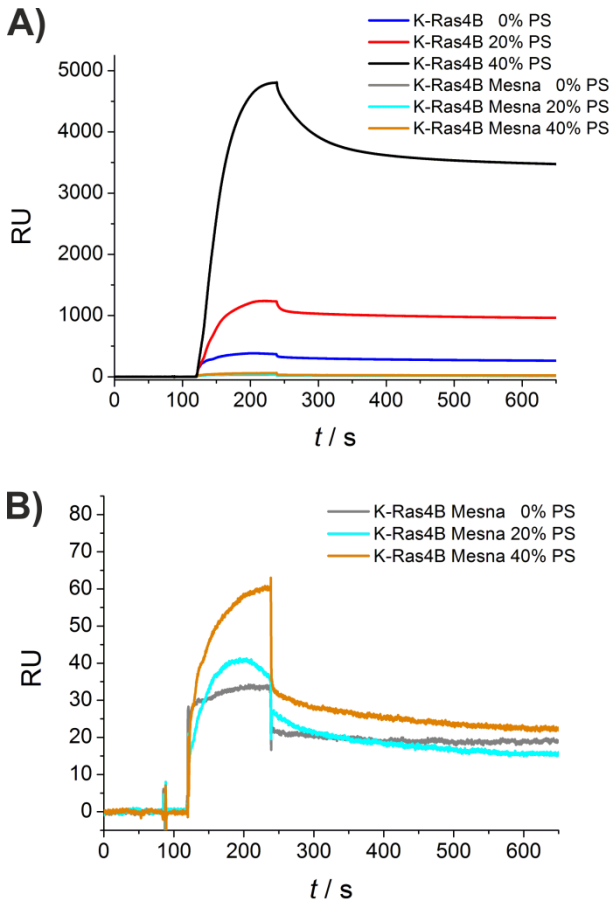

FIGURE S2 SPR sensorgrams of the binding of farnesylated and non-farnesylated, GDP-loaded K-Ras4B to lipid membranes consisting of POPC (0% PS), POPC/POPS 80:20 (20% PS), and POPC/POPS 60:40 (40% PS). (*A*) The sensorgrams clearly demonstrate a charge-dependent membrane binding of farnesylated K-Ras4B, whereas no significant membrane binding was observed for non-farnesylated K-Ras4B (termed K-Ras4B Mesna). (*B*) A detailed view also reveals no significant charge dependency for the membrane interaction of non-farnesylated K-Ras4B, contrary to the membrane interaction behavior of farnesylated K-Ras4B.

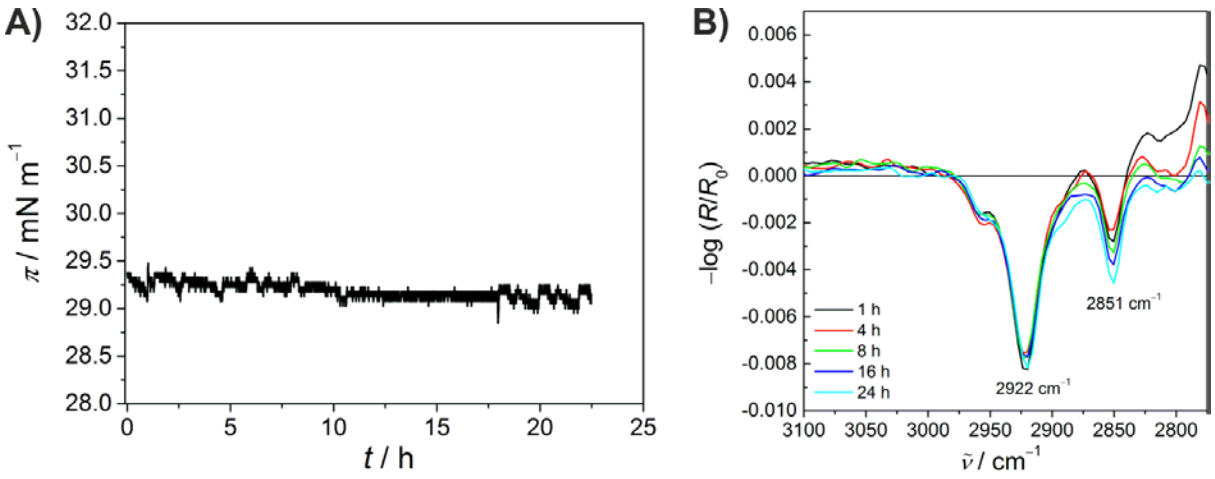

FIGURE S3 Long-term stability of the pure lipid monolayer film at the air-D_2O interface. (*A*) The surface pressure versus time course of the anionic raft-like lipid monolayer (DOPC/DOPG/DPPC/DPPG/Chol 20:5:45:5:25; molar ratio). The lipid film was spread at 29.5 mN m^{-1} at 20 °C. (*B*) IRRA spectra depicting the CH_2 asymmetric (at 2922 cm^{-1}) and symmetric (at 2851 cm^{-1}) vibrations of the lipid acyl chain region of the anionic lipid monolayer over a time period of 24 h. Both parameters remained essentially constant over the entire time period of the IRRAS experiment, implying long-term stability of the anionic lipid monolayer film. All IRRA spectra were acquired at 20 °C with p-polarized light at an angle of incidence of 35°.

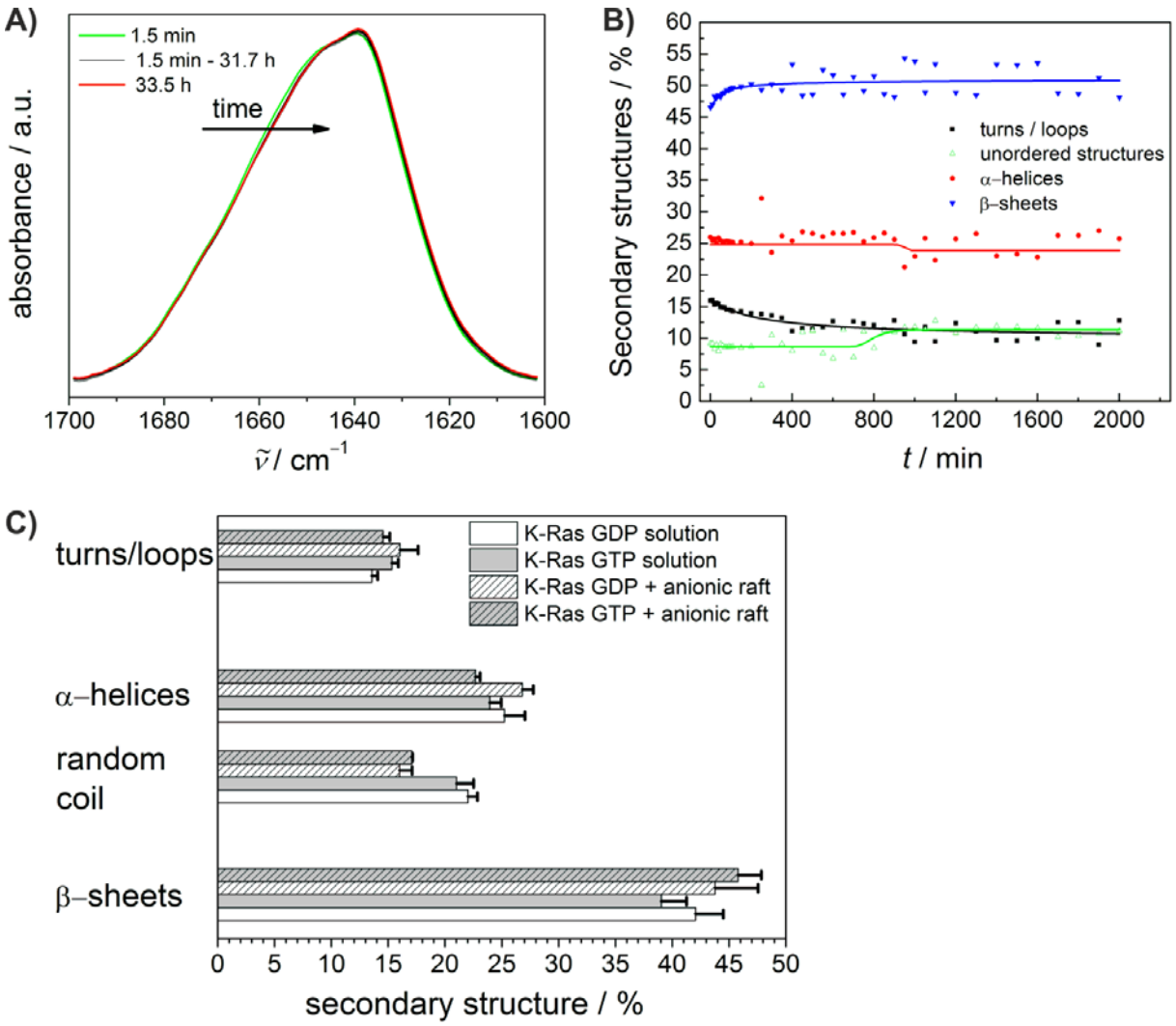

FIGURE S4 Long-term stability of GDP- and GTP-loaded K-Ras4B as analyzed by transmission FT-IR spectroscopy. (*A*) The normalized FTIR spectra for the time evolution of the amide-I′ band of K-Ras4B GTP in the presence of anionic lipid raft membranes composed of DOPC/DOPG/DPPC/DPPG/Chol 20:5:45:5:25 at 25 °C. (*B*) Temporal changes in the structure of K-Ras4B GTP upon interaction with anionic lipid raft bilayers. The secondary structure content was obtained by curve-fitting of the normalized amide-I′ band with a Boltzmann distribution function using the software Origin Pro 7.0. The goodness of fit was in the range of 99.2-99.6%. (*C*) Secondary structure contributions of K-Ras4B bound to different nucleotide states in bulk solution and upon interaction with anionic lipid raft vesicles at 25 °C. The concentration of each protein was 0.233 mM, with a protein to lipid ratio of 1:100. The results are an average of three experiments. The long-term stability of K-Ras4B proteins was ensured in the absence and presence of membranes by detecting no significant changes in secondary structure over the whole time range covered.

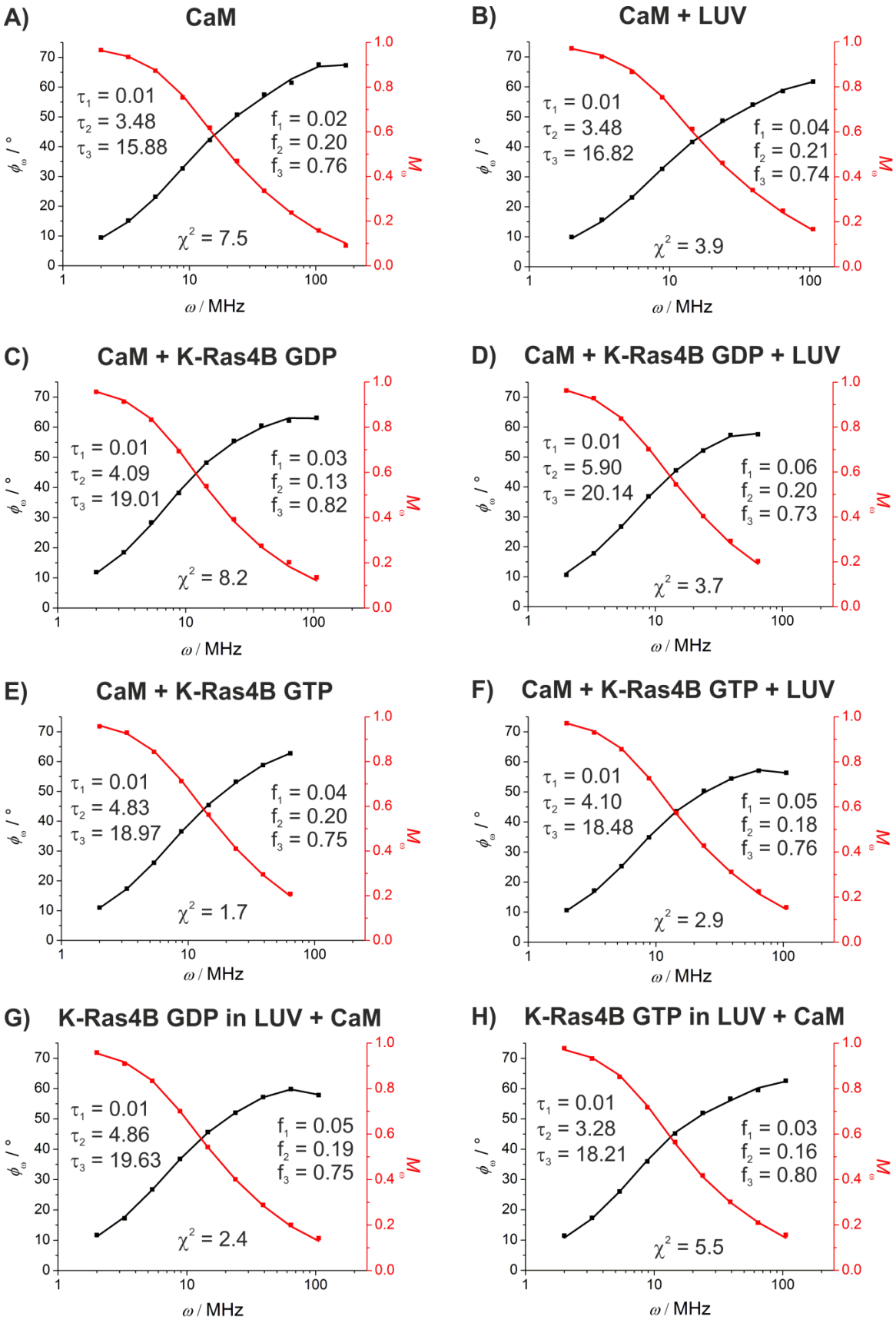

FIGURE S5 Representative phase angle, ϕ_{ϖ}, and modulation, M_{ϖ}, data for dansyl-labeled CaM under the different experimental conditions (black and red squares, respectively). The corresponding fits are shown as solid lines and all values are summarized in Table S1.

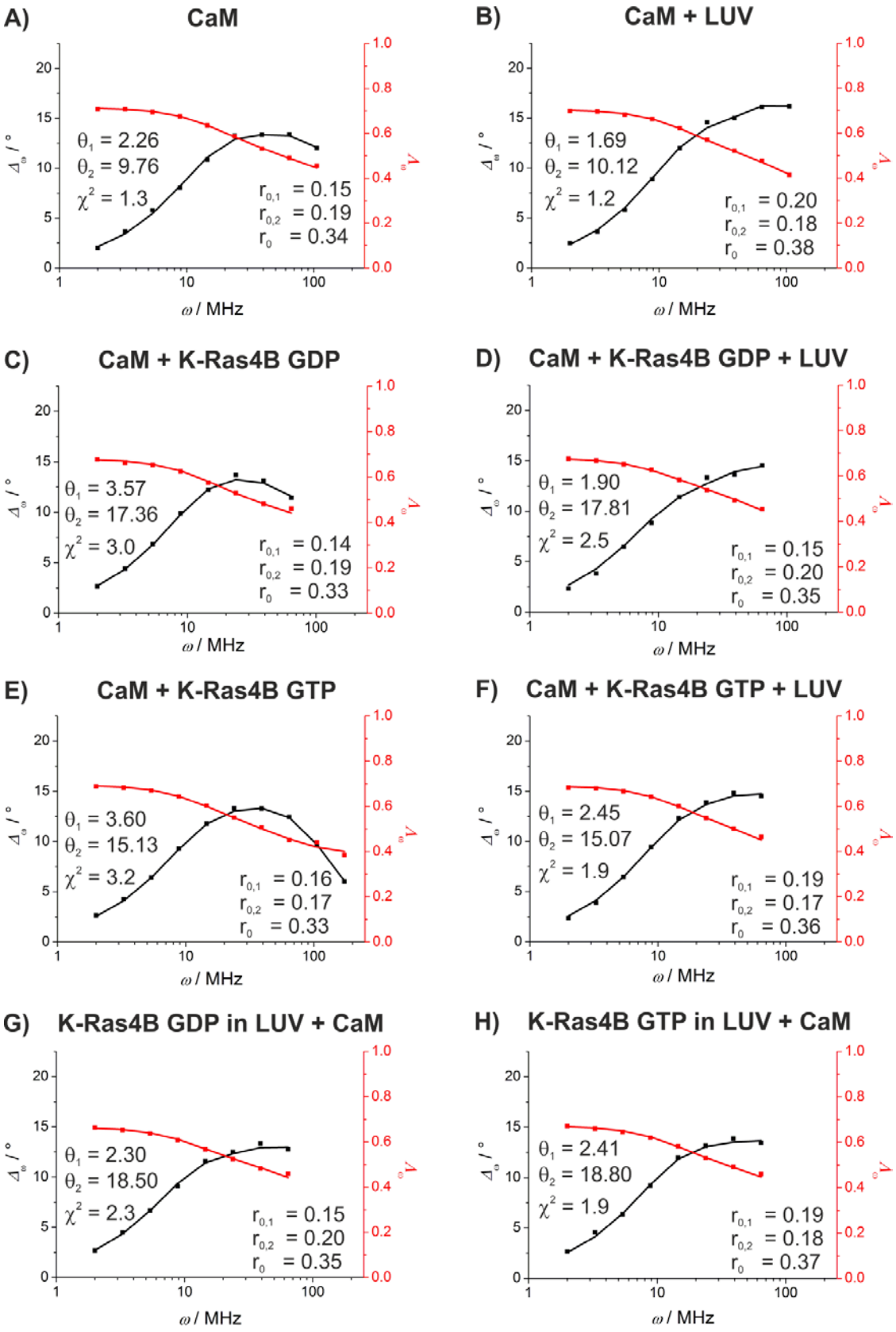

FIGURE S6 Representative differential phase, Δ_ω, and modulation ratio, Λ_ω, data for dansyl-labeled CaM under the different experimental conditions (black and red squares, respectively). The corresponding fits are shown as solid lines and all values are summarized in Table S2.

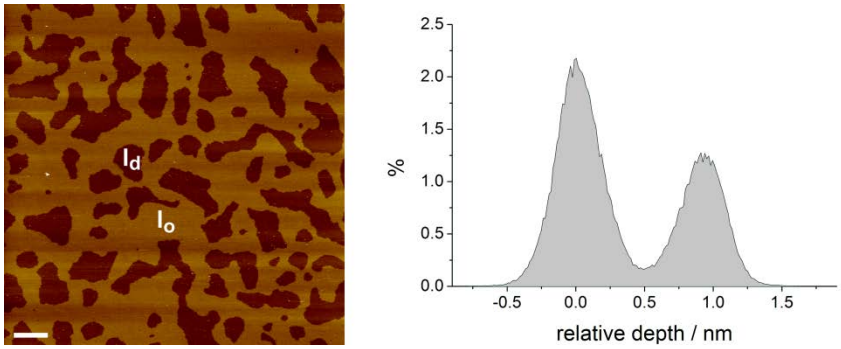

FIGURE S7 AFM image of a lipid membrane on mica consisting of DOPC/DOPG/DPPC/ DPPG/Chol 20:5:45:5:25 (mol%) before injection of protein solution into the AFM fluid cell. The scale bar corresponds to 1 μm. The depth histogram of the AFM image is shown on the right. The difference of the thickness between the l_d and l_o phase, determined from the AFM depth histogram, was 0.9 nm. Previous results confirmed a height difference between both phases of ~1 nm (2).

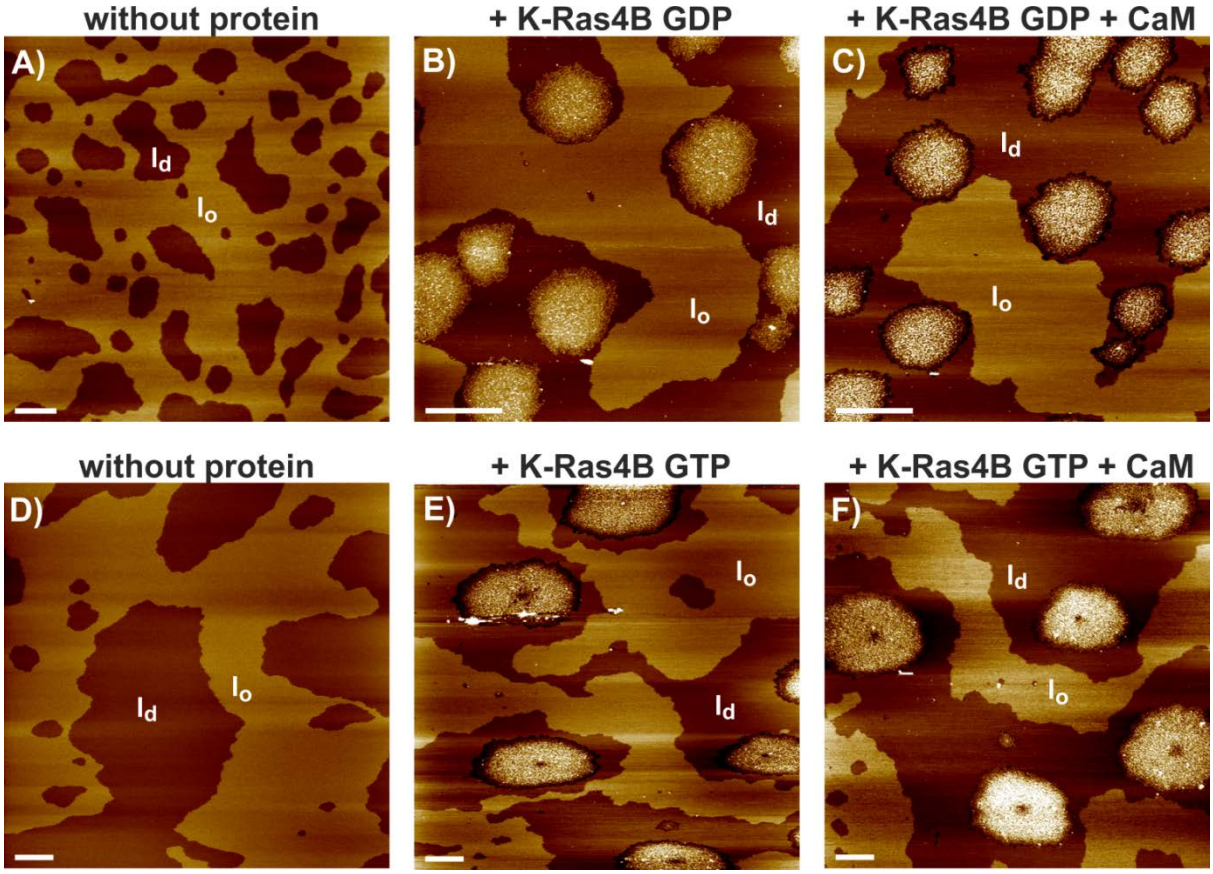

FIGURE S8 AFM images of the interaction of K-Ras4B GDP and K-Ras4B GTP with anionic raft membranes and subsequent addition of Ca^{2+}/CaM. Representative AFM images are shown before (panels *A* and *D*) and after injection of 800 μL K-Ras4B solution ($c_{K\text{-}Ras4B}$ = 0.2 μM) across the lipid membrane in the AFM fluid cell (panels *B* and *E*). After the formation of K-Ras4B-enriched domains in the l_d phase of the phase-separated membrane, a Ca^{2+}/CaM solution was injected into the AFM fluid cell (panels *C* and *F*) to study the effect of Ca^{2+}/CaM on membrane-bound K-Ras4B GDP/GTP. The overall height of the vertical color scale from dark brown to white corresponds to 8 nm for all images and the scale bar represents 1 μm.

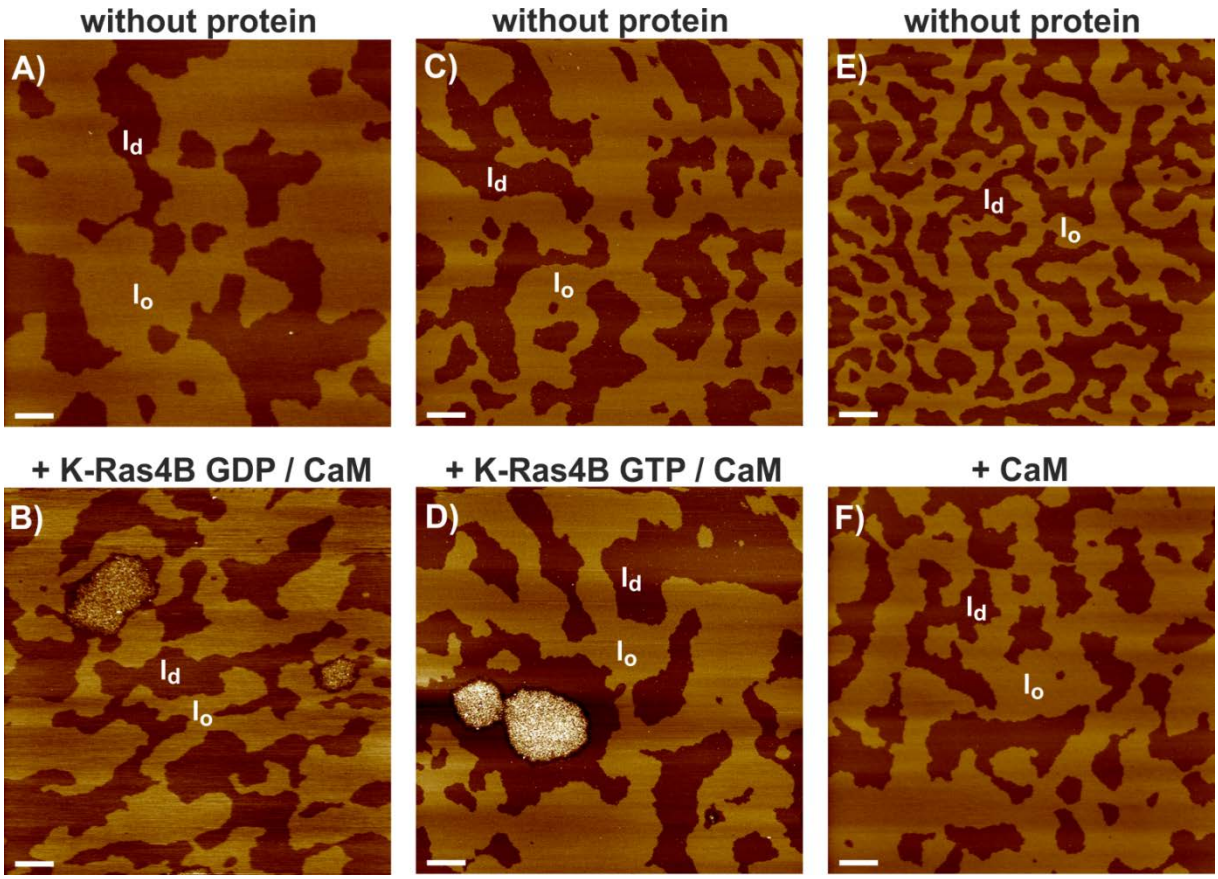

FIGURE S9 Effect of Ca^{2+}/CaM on the interaction of K-Ras4B GDP/GTP with anionic raft membranes. Representative AFM images are shown for the membrane interaction of the premixed K-Ras4B–Ca^{2+}/CaM complex (molar ratio 2:3) after ≈1 h of protein addition to the membrane (panel *B* and *D* for inactive and active K-Ras4B, respectively). Corresponding images before the addition of proteins are shown in panels (*A*) and (*C*). Panels (*E*) and (*F*) display representative AFM images of the anionic lipid raft membrane before and after injection of 800 μL Ca^{2+}/CaM (c = 0.3 μM) into the AFM fluid cell, respectively, indicating no membrane binding of Ca^{2+}/CaM. The overall height of the vertical color scale from dark brown to white corresponds to 8 nm for all images and the scale bar represents 1 μm.

TABLES

Table S1: Results of the fluorescence lifetime analysis. The fluorescence lifetimes τ_1 and τ_2 of dansyl-labeled, Ca^{2+}-loaded CaM and the corresponding fractional contributions f_1 and f_2 are given with the mean value ± standard deviation. Reduced χ^2 values were obtained in a range from 1 to 10.

	f_1	τ_1 / ns	f_2	τ_2 / ns	f_3	τ_3 / ns
CaM	0.03 ± 0.01	0.01	0.21 ± 0.02	3.50 ± 0.38	0.75 ± 0.02	15.93 ± 0.39
CaM + LUV	0.04 ± 0.00	0.01	0.22 ± 0.01	3.74 ± 0.35	0.73 ± 0.02	16.98 ± 0.33
CaM + K-Ras4B GDP	0.03 ± 0.01	0.01	0.17 ± 0.04	4.56 ± 1.16	0.78 ± 0.03	19.23 ± 1.27
CaM + K-Ras4B GTP	0.04 ± 0.01	0.01	0.19 ± 0.03	4.80 ± 0.65	0.76 ± 0.03	19.35 ± 0.56
CaM + K-Ras4B GDP + LUV	0.05 ± 0.01	0.01	0.20 ± 0.02	4.96 ± 0.95	0.74 ± 0.02	19.79 ± 0.71
CaM + K-Ras4B GTP + LUV	0.06 ± 0.02	0.01	0.21 ± 0.02	4.84 ± 1.22	0.73 ± 0.03	19.33 ± 0.85
K-Ras4B GDP in LUV + CaM	0.04 ± 0.02	0.01	0.19 ± 0.03	4.06 ± 1.33	0.77 ± 0.04	19.30 ± 0.65
K-Ras4B GTP in LUV + CaM	0.03 ± 0.01	0.01	0.17 ± 0.02	3.35 ± 0.38	0.79 ± 0.02	18.44 ± 0.52

Table S2: Results of the fluorescence anisotropy analysis. Rotational correlation times θ_1 and θ_2 (with θ_2 being equal to the overall rotational correlation time of the protein, i.e., $\theta_2 = \theta_{\text{dansyl-CaM}}$) of danysl-labeled, Ca^{2+}-loaded CaM and corresponding values for $r_{0,1}$ and $r_{0,2}$ are shown with the mean value ± standard deviation. Reduced χ^2 values were obtained in a range from 0.3 to 5.4.

	$r_{0,1}$	θ_1 / ns	$r_{0,2}$	θ_2 / ns	r_0
CaM	0.15 ± 0.03	1.97 ± 0.54	0.20 ± 0.02	9.44 ± 0.87	0.35 ± 0.02
CaM + LUV	0.19 ± 0.06	1.87 ± 0.73	0.18 ± 0.06	10.13 ± 2.73	0.37 ± 0.01
CaM + K-Ras4B GDP	0.15 ± 0.02	3.62 ± 0.60	0.19 ± 0.02	17.87 ± 1.29	0.33 ± 0.01
CaM + K-Ras4B GTP	0.15 ± 0.02	3.68 ± 0.69	0.18 ± 0.02	16.06 ± 2.09	0.33 ± 0.01
CaM + K-Ras4B GDP + LUV	0.19 ± 0.03	2.22 ± 0.60	0.17 ± 0.02	18.01 ± 2.30	0.36 ± 0.01
CaM + K-Ras4B GTP + LUV	0.18 ± 0.03	2.26 ± 0.72	0.18 ± 0.03	16.26 ± 1.70	0.36 ± 0.01
K-Ras4B GDP in LUV + CaM	0.16 ± 0.01	2.47 ± 0.77	0.20 ± 0.02	18.38 ± 0.55	0.36 ± 0.02
K-Ras4B GTP in LUV + CaM	0.19 ± 0.01	2.41 ± 0.58	0.18 ± 0.02	18.30 ± 1.72	0.36 ± 0.02

SUPPORTING REFERENCES

1. Weise, K., S. Kapoor, A. Werkmüller, S. Möbitz, G. Zimmermann, G. Triola, H. Waldmann, and R. Winter. 2012. Dissociation of the K-Ras4B/PDEδ Complex upon Contact with Lipid Membranes: Membrane Delivery Instead of Extraction. *J. Am. Chem. Soc.* 134:11503–11510.
2. Weise, K., S. Kapoor, C. Denter, J. Nikolaus, N. Opitz, S. Koch, G. Triola, A. Herrmann, H. Waldmann, and R. Winter. 2011. Membrane-Mediated Induction and Sorting of K-Ras Microdomain Signaling Platforms. *J. Am. Chem. Soc.* 133:880–887.
3. Gohlke, A., G. Triola, H. Waldmann, and R. Winter. 2010. Influence of the Lipid Anchor Motif of N-Ras on the Interaction with Lipid Membranes: A Surface Plasmon Resonance Study. *Biophys. J.* 98:2226–2235.
4. Kapoor, S., G. Triola, I. R. Vetter, M. Erlkamp, H. Waldmann, and R. Winter. 2012. Revealing conformational substates of lipidated N-Ras protein by pressure modulation. *Proc. Natl. Acad. Sci. USA.* 109:460–465.
5. Gratton, E., and M. Limkeman. 1983. A continuously variable frequency cross-correlation phase fluorometer with picosecond resolution. *Biophys. J.* 44:315–324.
6. Gratton, E., D. M. Jameson, and R. D. Hall. 1984. Multifrequency phase and modulation fluorometry. *Annu. Rev. Biophys. Bioeng.* 13:105–124.
7. Yao, Y., C. Schoneich, and T. C. Squier. 1994. Resolution of structural changes associated with calcium activation of calmodulin using frequency domain fluorescence spectroscopy. *Biochemistry.* 33:7797–7810.
8. Kapoor, S., A. Werkmüller, C. Denter, Y. Zhai, J. Markgraf, K. Weise, N. Opitz, and R. Winter. 2011. Temperature-pressure phase diagram of a heterogeneous anionic model biomembrane system: results from a combined calorimetry, spectroscopy and microscopy study. *Biochim. Biophys. Acta.* 1808:1187–1195.
9. Evers, F., C. Jeworrek, K. Weise, M. Tolan, and R. Winter. 2012. Detection of lipid raft domains in neutral and anionic Langmuir monolayers and bilayers of complex lipid composition. *Soft Matter.* 8:2170–2175.
10. Humphrey, W., Dalke, A. and Schulten, K. 1996. VMD - Visual Molecular Dynamics. *J. Molec. Graphics.* 14:33–38.